Supporting information

Quantitative structural analysis of binary nanocrystal superlattices by electron tomography

Heiner Friedrich[1], Cedric J. Gommes[2], Karin Overgaag[3‡], Johannes D. Meeldijk[4], Wiel H. Evers[3], Bart de Nijs[3], Mark P. Boneschanscher[3], Petra E. de Jongh[1], Arie J. Verkleij[4], Krijn P. de Jong[1], Alfons van Blaaderen[5] and Daniel Vanmaekelbergh[3]

[1] Inorganic Chemistry and Catalysis, Debye Institute for Nanomaterials Science, Utrecht University, Sorbonnelan 16, Utrecht 3584 CA, The Netherlands

[2] Department of Chemical Engineering, University of Liège, Allée du 6 août 3, 4000 Liège, Belgium

[3] Condensed Matter and Interfaces, Debye Institute for Nanomaterials Science, Utrecht University, Princetonplein 1, Utrecht 3584 CC, The Netherlands

[4] Electron Microscopy Group, Utrecht University, Padualaan 8, Utrecht 3584 CH, The Netherlands

[5] Soft Condensed Matter, Debye Institute for Nanomaterials Science, Utrecht University, Princetonplein 1, Utrecht 3584 CC, The Netherlands

‡ Present address: Shell International E&P, Postbus 80, 2280 AB Rijswijk, The Netherlands.

The supporting information section was organized following the order of data presentation in the manuscript. For easy access to individual sections of this document please refer to the table of content shown below. In addition please consult the supporting media files showing the aligned tilt-series (SImovie1.mpg) and the corresponding reconstruction (SImovie2.mpg) of the AB_{13} superlattice.

Table of content

The overall quantification of the electron tomograms encompassed two steps: (i) image analysis aiming at extracting the position and size of all nanoparticles in the reconstructed volume, and (ii) analysis of the particle positions and sizes in terms of lattice parameters, crystal structure and nearest neighbor distances. Structure and image analysis were carried out in Matlab 7.4 (The MathWorks, Inc.).

Image analysis

Image analysis proceeded in three steps. First, the position of all particles was obtained by template matching.[21] Templates were defined as spherical dark regions (of value -1), surrounded by a bright shell (of value +1). This template model corresponds well with the appearance of the NC in the tomogram exposing dark cores and a bright rim. The bright rim results from underfocus condition during acquisition as well as the reconstruction point spread function. Templates were normalized so that the sum of all intensities in the template is zero. Normalization ensures a response of zero in a region of uniform intensity. The criterion for particle detection is a correlation larger than 0.5 between template and reconstruction.[22] To account for dispersion in the particle size distribution templates of variable size were employed. The centroids of the correlation peaks (> 0.5) are considered as the position of the particle. In the second step of image analysis the radius of the particles was determined. For each particle, the image intensity was radially averaged over the three horizontal slices closest to the particle center. The radial intensity average shows a distinct edge-like profile, going from low values in the center region (dark core) and increasing dramatically to high values in the shell region (bright rim). The radius of the particle is determined as the radial distance at which the intensity is exactly halfway between the minimum and maximum.[23] The third and final step of image analysis removed false positives. Four independent criteria are applied based on contrast, average intensity, size, and position to ensure proper detection for both NC classes independently. The presented methodology enabled us to characterize thousands of NC in each tomogram containing less than 5 % false positives for high-contrast PbSe and Au NC and around 10% false positives for the low-contrast CdSe NC. We estimate that, overall, approximately 90 % of the NCs were detected.

Structure analysis

While image analysis provided the position and radius of the individual NC in the reconstruction, this section deals with extracting the crystal structure from the data. To detect local variations, structure analysis was performed on multiple sub-regions of the tomogram as indicated in Figure SI 1. In a step preceding structure analysis, NC core diameters (d_{core}) were fitted assuming a Gaussian spread (see SI Table 1 to 4). In addition, the average soft shell thickness was calculated by subtracting the two NC core radii from their respective distance. The values presented in SI Table 1 to 4 take either the minimum soft shell thickness (t_{min}, nearest neighbour only) or an average over the three smallest soft shell thicknesses (t_{3NN}, three nearest neigbours) into account. Structure analysis included four successive steps, as explained hereafter.

Detection of crystalline clusters of particles.

First, a 3-dimensional Voronoi tessellation is performed on the PbSe NC data in order to detect which particles are first neighbors to each other. The Voronoi tessellation divides space into cells defined as the locus of all points closer to a given particle than to any other. Two particles are then said to be neighbors if their Voronoi cells touch each other. Following other studies,[24-26] the rotational symmetry of the configuration of closest neighbors to any particle is quantified using spherical harmonics with $l = 6$. For any particle i, we calculate

$$q_{6m}(i) = \frac{1}{B} \sum_{n=1}^{N_i} Y_{6m}(\hat{r}_{in}) \tag{1}$$

where $\hat{r}_{in}$ is the unit vector pointing from particle i to its nth neighbor, N_i is the number of neighbors to particle i, Y_{6m} are the spherical harmonics with $l = 6$, and B is normalizing constant chosen so that:

$$\sum_{m=-6}^{6} q^{*}_{6m}(i) q_{6m}(i) = 1$$

The rotational invariant Q_6 is calculated for each particle as

$$Q_6(i) = \sqrt{\frac{4\pi}{13} \sum_{m=-6}^{6} |q_{6m}(i)|^2} \tag{2}$$

serving as a measure of the crystallinity around particle i. The particle having the largest value of Q_6 is found, corresponding to number i_{max}.

To find the set of other particles that belong to same crystallite as particle i_{max}, we calculate the complex inner product

$$C_q(i_{max}, j) = \sum_{m=-6}^{+6} q_{6m}(i_{max}) q^*_{6m}(j) \qquad (3)$$

which is an objective measure of the similarity in rotational symmetry around particle j and particle i_{max}. The crystallite containing particle i_{max} is defined as the set of all touching particles with $C_q(i_{max},j) > 0.5$. As $C_q(i_{max},i_{max}) = 1$, because of the normalization constant B in Equation 1, this cluster of particles necessarily contains i_{max}.

Determination of the crystallite lattice parameters.

When the detected crystalline cluster contains more than 50 particles, its structure is analyzed as follows. The crystalline cluster generally contains some holes, meaning that some of its particles are not detected. Before analyzing the structure, the holes have to be filled. For that purpose, letting $\mathbf{x}_n$ be the 3-dimensionnal positions of the particles in the cluster, the function F($\mathbf{x}$) is defined as

$$F(\mathbf{x}) = \sum_{c=1}^{N} \sum_{n=1}^{N} G_\sigma\left(\left\|\mathbf{x} - (\mathbf{x}_n - \mathbf{x}_c)\right\|\right) \qquad (4)$$

where G_σ is a Gaussian with standard deviation σ. Equation 4 takes successively every particle of the cluster as the origin (sum over index c), and it creates a Gaussian function centered on the position of all other particles (sum over n) with respect to particle c. The maxima of function F are therefore expected to have the same translational symmetry as the cluster, with the gaps filled. Another advantage of using Equation 4 is that no particle is given a preferential role in the analysis. In practice, σ is chosen equal to the average particle radius.

The purpose is now to find the crystal structure. Let x(n), y(n) and z(n) be the coordinates of the nth maximum of function F($\mathbf{x}$ = [x, y, z]). The relation between the lattice base vectors ($\mathbf{a}$, $\mathbf{b}$, $\mathbf{c}$) and the positions of the lattice points can be written in the matrix form

$$\begin{pmatrix} x(1) & y(1) & z(1) \\ \vdots & \vdots & \vdots \\ x(N) & y(N) & z(N) \end{pmatrix} = \begin{pmatrix} 1 & K(1) & L(1) & M(1) \\ \vdots & \vdots & \vdots & \vdots \\ 1 & K(n) & L(n) & M(n) \end{pmatrix} \begin{pmatrix} x_0 & y_0 & z_0 \\ a_x & a_y & a_z \\ b_x & b_y & b_z \\ b_x & c_y & c_z \end{pmatrix} \qquad (5)$$

where K(n), L(n), M(n) are the lattice indices, and (x_0, y_0, z_0) is the position of the origin. If the indices were known, Equation 5 would be a linear over-determined system, which could be solved in the least-square sense for the base vectors and the position of the origin. The problem is solved in two steps. First, the position of the 3 maxima of F(x) which are the closest to x = 0 are chosen as a first guess of the base vectors. After defining a suitable lattice based on linear combinations of the 'guess' base vectors, the indices K, L, M of each particle are calculated. Second, using these indices, Equation 5 is solved in the least-square sense to provide the final value of the base vectors.

## Completing the crystallites based on its lattice parameters.

Once the lattice parameters of a crystallite are known, the expected positions of all particles belonging to it is calculated from Equation 5, with K, L, M taking all possible integer values. The initial crystalline cluster considered in section 1 is then grown progressively, by adding one by one any particle that touches and that is close enough to a lattice node. At this stage, all particles that have already been assigned to a given crystallite are excluded from further analysis and step 1 is then repeated, starting from the remaining particle with the largest value of Q_6 to find additional crystalline regions.

The length and relative angles of lattice vectors are provided in SI Table 1 to 4. Subsequently, the unit cell filling fractions and NC size ratios were calculated based on particle size, soft shell thickness, unit cell vector length. These results (SI Table 1 to 4) illustrate that filling fractions and particle size ratios vary dramatically between the hard core and the different hard core plus soft shell approximations.

Statistical analysis of the unit cell.

Based on the PbSe lattice points and vectors belonging to individual crystalline regions additional NC (CdSe, Au, PbSe) within the unit cell (UC) were analysed with respect to their average position. Since not all NC within the lattice could be detected the statistical analysis was performed on arrangements having 7-8 PbSe NC in the eight corners of the UC and 1-2 CdSe or Au for AB_2, 12-13 CdSe for AB_{13} and 3-4 Au + 1-2 PbSe for AB stoichiometries. The average lattice positions, for additional NC within the UC, were determined by k-means clustering and are provided in SI Table 1 to 4. The fact that average crystallographic information can be provided independent of lattice contractions highlights again the versatility of the presented methodology.

Figure SI 1
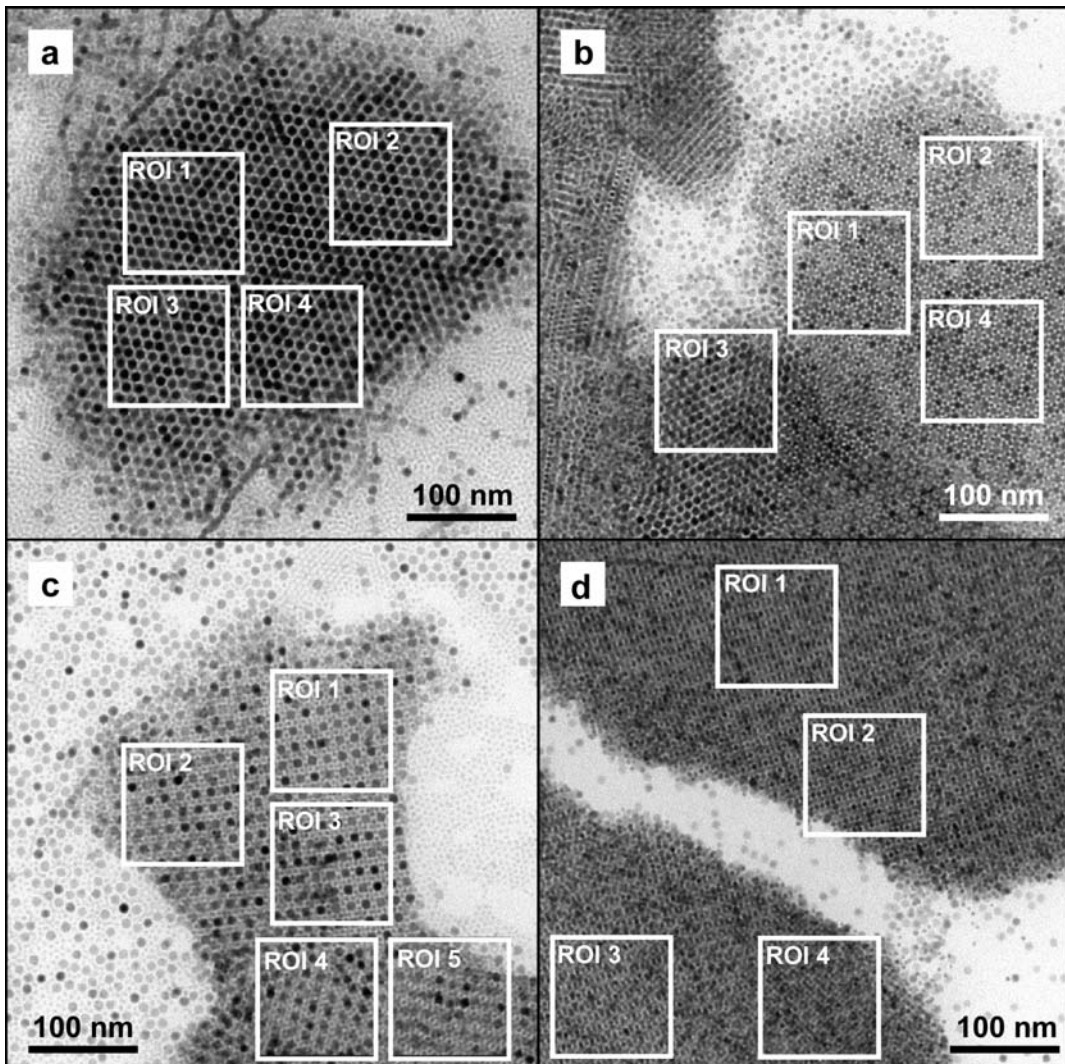
Figure SI 1. TEM images of examined superlattices at zero tilt and regions of interest (ROI) which were analyzed in terms of particle size, soft shell thickness, unit cell vectors and angles, and underlying crystallographic lattice. (a) AB_2 consisting of PbSe and CdSe NCs, (b) AB_2 consisting of PbSe and Au NCs, (c) AB_{13} consisting of PbSe and CdSe NCs, and (d) AB consisting of PbSe and Au NC.

Figure SI 2
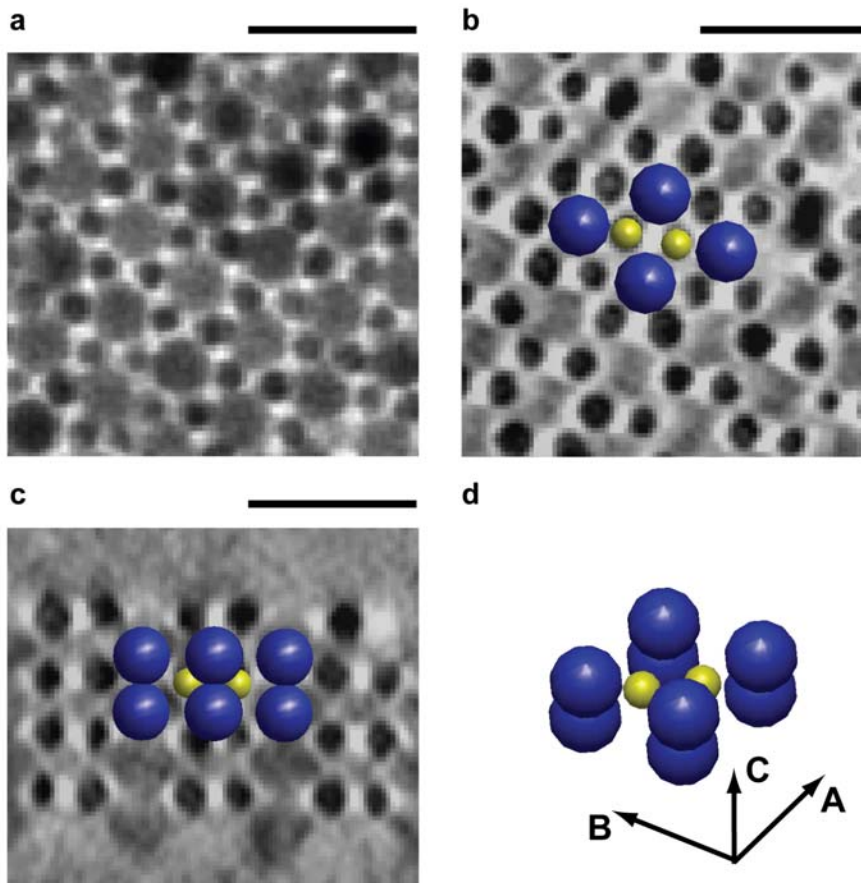
Figure SI 2. Crystallographic analysis of AB_2 superlattice consisting of 7.1 nm PbSe and 3.7 nm Au NCs. (a) TEM image along (001) direction at zero tilt, (b) numerical cross-section parallel to [001] plane through Au NCs, (c) cross-section parallel to [1-10] plane through PbSe and Au NCs, (d) 3D representation of the average unit cell which is isostructural with AlB_2 (space group 191) showing PbSe NCs in blue and Au NCs in yellow. Scale bars are 20 nm.

Figure SI 3
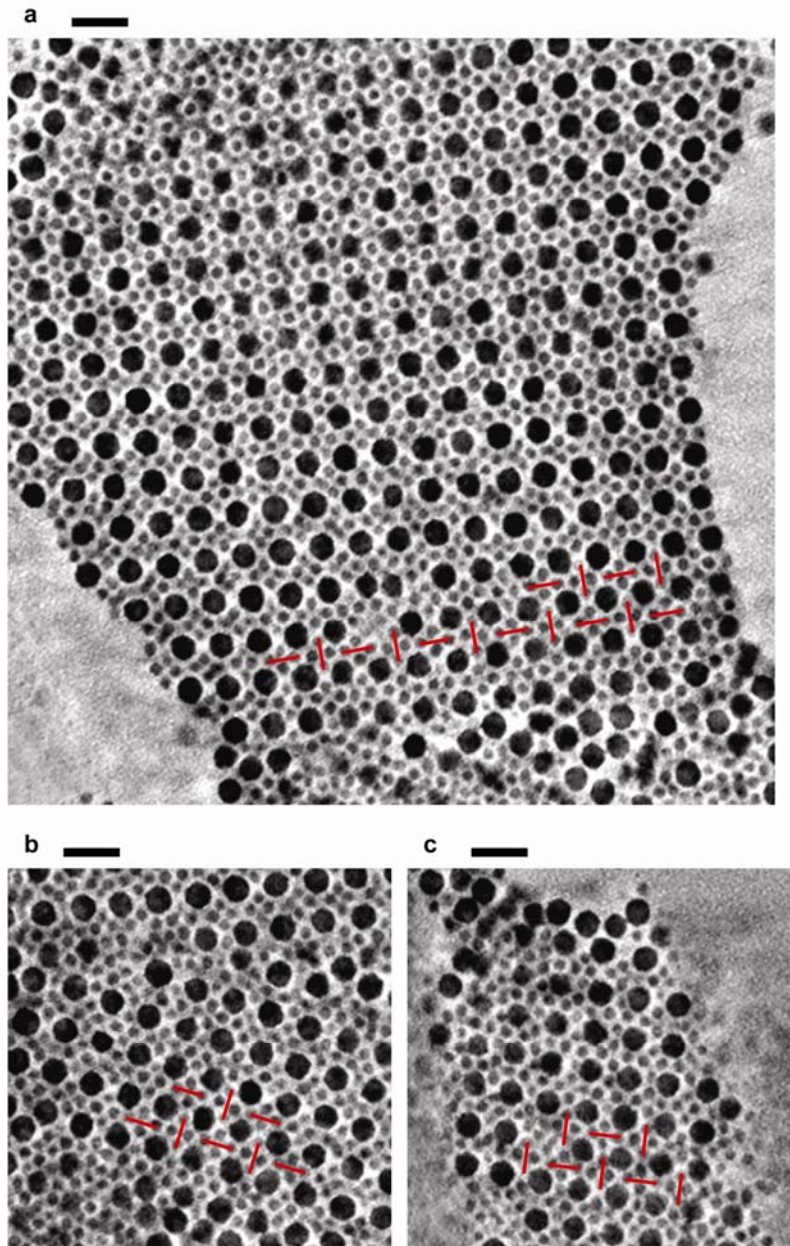
Figure SI 3. Numerical cross-sections (interpolated from 0.54 nm/px) parallel to the [001] lattice planes of AB_{13} lattices composed of PbSe and CdSe NCs. The cross-sections slice through the PbSe and the four CdSe closest to the [001] lattice plane. (a) crystallite in ROI 1 to 3, (b) crystallite in ROI 4, and (c) crystallite in ROI 5. As a visual guide the elongation of the CdSe quadrangle, alternating by 90° between neighbouring cells, is indicated by red lines. Scale bars are 20 nm.

Figure SI 4
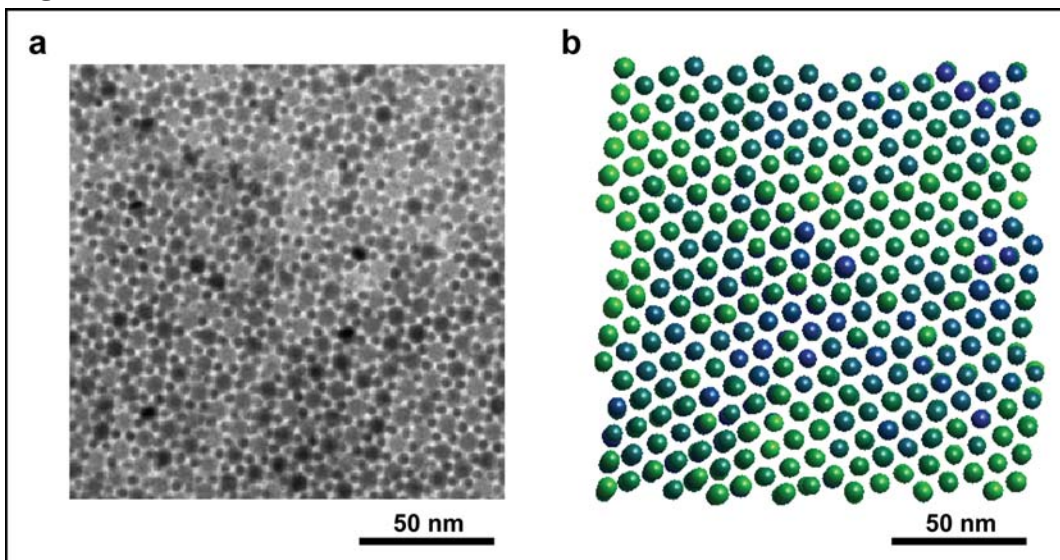
Figure SI 4. (a) TEM image (along (001) direction at zero tilt) of AB_2 superlattice consisting of PbSe and Au NCs, and (b) displacement map of same region with PbSe NCs color coded from blue to green depending on their distance to the next lattice point. PbSe in blue are on the lattice and PbSe that are 2.5 nm off their respective lattice position are shown in green. It is evident that the displacements become larger closer to the left and bottom boundary of the region which we attribute to an overall bending of the superlattice.

Figure SI 5
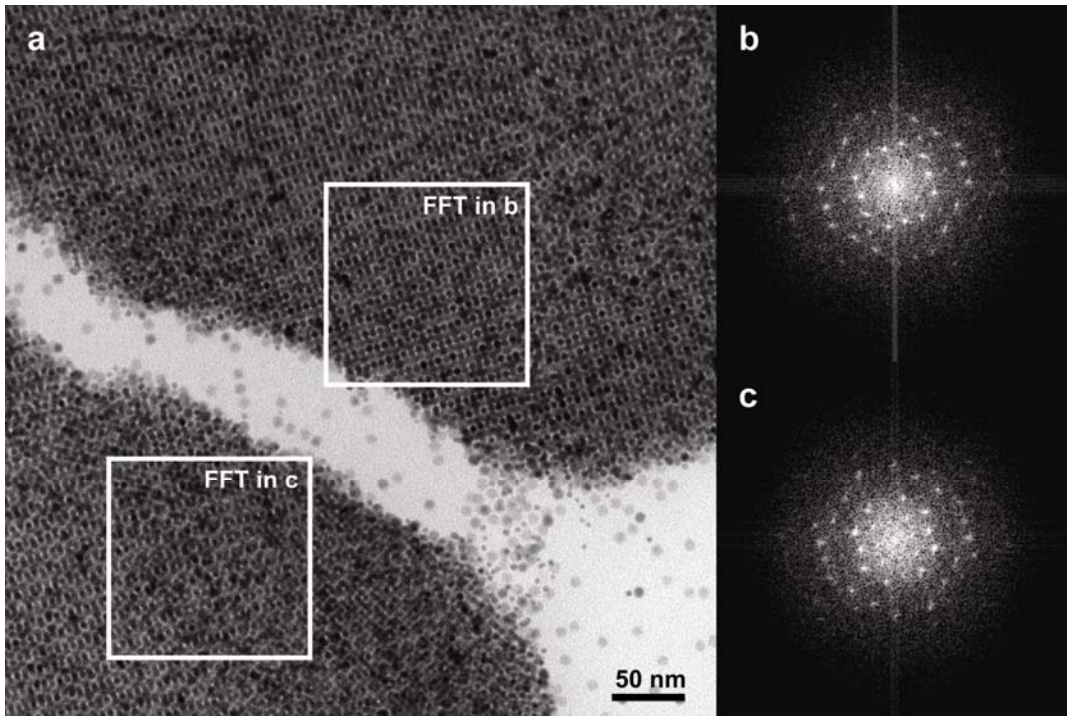
Figure SI 5 (a) TEM image (along (010)direction at zero tilt) of AB superlattice composed of PbSe and Au NCs. (b,c) Fast Fourier Transforms (FFT) of indicated regions illustrate the underlying periodicity.

Figure SI 6
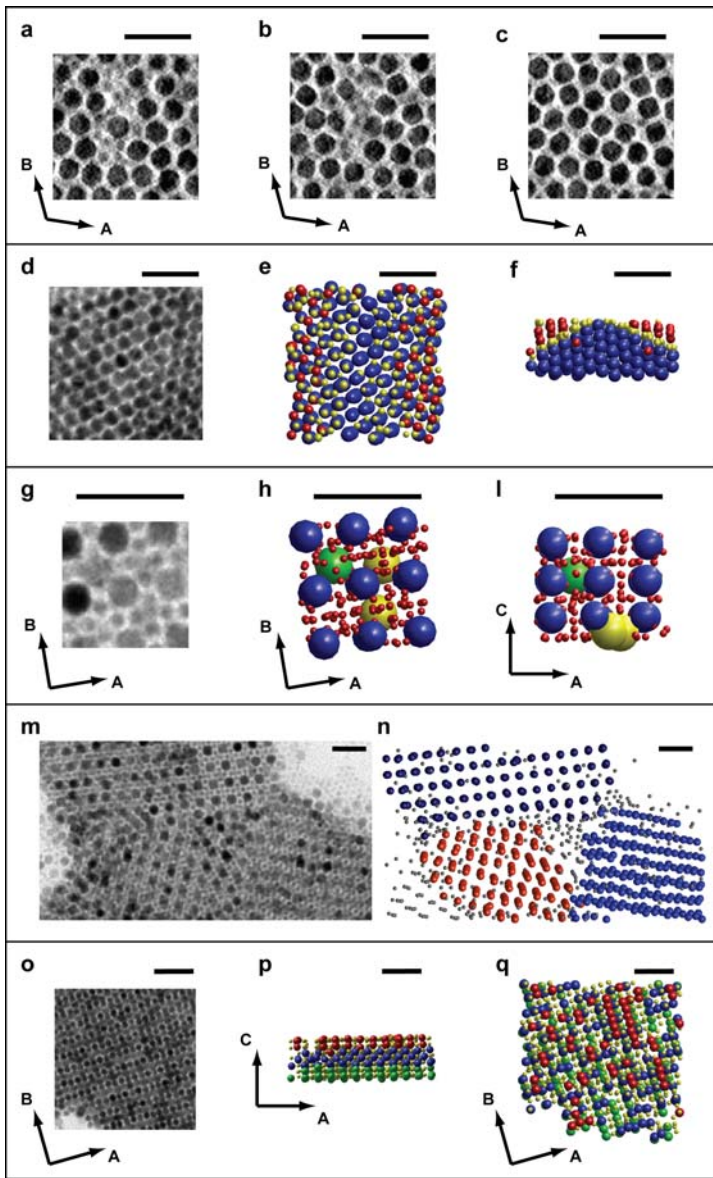
Figure SI 6. Examples of lattice defects in binary nanoparticle superlattices with AB_2, AB_{13} and AB stoichiometry. (a-c) ET slices through AB_2 consisting of PbSe and CdSe NCs showing disorder/order transition between first (a), second (b) and third (c) PbSe layer from surface.

(d-f) demixed region (ROI 4 in Fig. SI 1b) in AB_2 of PbSe and Au NCs with (d) TEM image, (e,f) ET analysis showing demixed PbSe pyramid in blue, additional PbSe in red and Au in yellow. (g-l) AB_{13} of PbSe and CdSe NCs with (g) TEM image, (h,l) ET analysis showing PbSe in blue, CdSe in red, intracrystalline PbSe in green and surface-adsorbed PbSe in yellow. (m,n) intergrowth of multiple AB_{13} crystallites consisting of PbSe and CdSe NCs with (m) TEM image, (n) ET analysis showing three PbSe lattices in black, blue, orange, and PbSe off lattice in gray. (o-q) grain boundaries in AB consisting of PbSe and Au NCs with (o) TEM image, (p,q) ET analysis showing PbSe belonging to different crystallites, i.e. different layers in green, blue, red and Au NC in yellow. Scale bars are 30 nm.

13
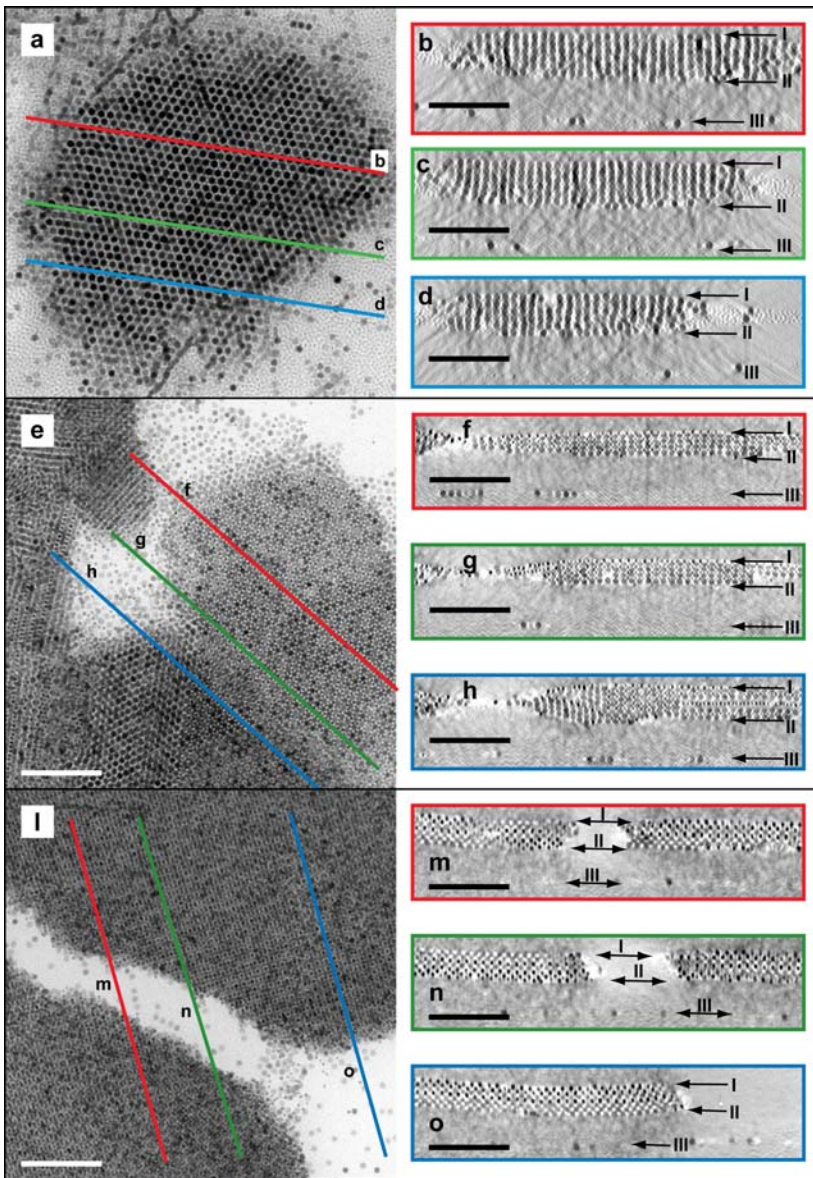
Figure SI 7. Analysis of the top and bottom surfaces in AB and AB_2 superlattices showing TEM images (a,e,l) and numerical cross-sections perpendicular to the support (b-d,f-h,m-o). The position of the perpendicular cross-section is indicated by colored lines in the TEM images. The top of the sections corresponds to the suspension/air interface (I), and the bottom to the suspension/support interface (II). The third surface (III) was identified as the back side of the polymer support film. (a-d) AB_2 consisting of PbSe and CdSe NCs, (e-h) AB_2 consisting of PbSe and Au NCs, (l-o) AB consisting of PbSe and Au NCs. Scale bars are 100 nm.

SI Table 1 ET analysis of AB$_2$ consisting of PbSe and CdSe NCs.

Particle size distribution and shell thickness (normal distribution) in nm

Region	PbSe d$_{core}$	PbSe t$_{min}$	PbSe t$_{3NN}$	CdSe d$_{core}$	CdSe t$_{min}$	CdSe t$_{3NN}$
ROI 1	9.0±0.3	-0.3±0.7*	0.5±0.5	3.4±0.5	1.1±0.4	1.4±0.3
ROI 2	9.0±0.3	-0.4±0.9*	0.5±0.6	3.4±0.5	1.2±0.4	1.5±0.3
ROI 3	9.0±0.3	-0.4±0.7*	0.5±0.5	3.4±0.5	1.1±0.3	1.5±0.2
ROI 4	9.0±0.3	-0.4±0.7*	0.5±0.6	3.3±0.5	1.1±0.4	1.4±0.3

Unit cell vector length and average displacement (rms) from lattice in nm

Region	A [nm]	B [nm]	C [nm]	Volume [nm³]
ROI 1	11.2±0.8	11.7±0.6	8.4±1.0	956
ROI 2	11.6±0.7	11.4±0.7	8.4±0.9	982
ROI 3	11.2±0.7	11.5±0.6	8.4±0.9	970
ROI 4	11.4±0.6	11.7±0.6	8.0±1.1	928

Unit cell vector angles in degrees

Region	AB [°]	BC [°]	CA [°]
ROI 1	119.9	91.7	88.8
ROI 2	117.8	90.0	90.5
ROI 3	116.2	91.1	88.5
ROI 4	118.4	86.4	90.3

Unit cell filling fractions (ρ) and size ratios (γ)

Region	ρ(d$_{core}$)	ρ(d$_{core}$+t$_{min}$)	ρ (d$_{core}$+t$_{3NN}$)	γ (d$_{core}$)	γ (d$_{core}$+t$_{min}$)	γ (d$_{core}$+t$_{3NN}$)
ROI 1	0.439	0.451	0.586	0.379	0.517	0.508
ROI 2	0.428	0.439	0.584	0.376	0.533	0.512
ROI 3	0.436	0.448	0.587	0.374	0.520	0.507
ROI 4	0.458	0.466	0.614	0.368	0.512	0.497

CdSe position (mean±std) in unit cell of ROI 2 expressed in multiples of A,B,C

	A	B	C
CdSe 1	0.34±0.05	0.69±0.06	0.51±0.11
CdSe 2	0.63±0.05	0.28±0.06	0.49±0.09

* A negative minimum neighbor distance (t$_{min}$) which could be interpreted as penetration of the NC hard cores is unphysical. Instead it results from analyzing NC as spherical objects which only approximates the actual shape of a faceted crystallite.

SI Table 2 ET analysis of AB$_2$ consisting of PbSe and Au NCs.

Particle size distribution and shell thickness (normal distribution) in nm

Region	PbSe d_{core}	PbSe t_{min}	PbSe t_{3NN}	Au d_{core}	Au t_{min}	Au t_{3NN}
ROI 1	7.1±0.4	0.2±0.7*	0.8±0.5	3.7±0.4	0.9±0.3	1.2±0.2
ROI 2	7.1±0.4	-0.2±0.7*	0.5±0.5	3.7±0.4	0.9±0.3	1.2±0.2
ROI 3	7.1±0.4	0.1±0.7*	0.7±0.5	3.7±0.4	0.9±0.3	1.2±0.3

Unit cell vector length and average displacement (rms) from lattice in nm

Region	A [nm]	B [nm]	C [nm]	Volume [nm³]
ROI 1	9.8±0.4	10.1±0.4	7.2±0.5	630
ROI 2	10.2±1.1	10.3±0.9	6.5±0.7	594
ROI 3	9.9±0.4	10.0±0.4	6.7±0.8	581

Unit cell vector angles in degrees

Region	AB [°]	BC [°]	CA [°]
ROI 1	117.5	90.1	91.9
ROI 2	119.6	90.1	91.2
ROI 3	117.8	90.4	90.4

Unit cell filling fractions (ρ) and size ratios (γ)

Region	$\rho(d_{core})$	$\rho(d_{core}+t_{min})$	$\rho(d_{core}+t_{3NN})$	$\gamma(d_{core})$	$\gamma(d_{core}+t_{min})$	$\gamma(d_{core}+t_{3NN})$
ROI 1	0.388	0.502	0.616	0.524	0.633	0.628
ROI 2	0.408	0.469	0.593	0.525	0.662	0.641
ROI 3	0.410	0.506	0.626	0.522	0.645	0.634

Au position (mean±std) in unit cell of ROI 3 expressed in multiples of A,B,C

	A	B	C
Au 1	0.33±0.05	0.68±0.05	0.52±0.08
Au 2	0.65±0.05	0.32±0.05	0.51±0.09

* A negative minimum neighbor distance (t_{min}) which could be interpreted as penetration of the NC hard cores is unphysical. Instead it results from analyzing NC as spherical objects which only approximates the actual shape of a faceted crystallite.

SI Table 3 ET analysis of AB$_{13}$ consisting of PbSe and CdSe NCs.

Particle size distribution and shell thickness (normal distribution) in nm

Region	PbSe d$_{core}$	PbSe t$_{min}$	PbSe t$_{3NN}$	CdSe d$_{core}$	CdSe t$_{min}$	CdSe t$_{3NN}$
ROI 1	8.8±0.3	0.1±0.7*	0.5±0.4	3.8±0.4	0.6±0.5	0.9±0.3
ROI 2	8.8±0.3	0.2±0.4*	0.5±0.3	3.8±0.4	0.6±0.4	0.9±0.3
ROI 3	8.8±0.3	0.1±0.4*	0.4±0.3	3.8±0.4	0.5±0.4	0.9±0.3
ROI 4	8.7±0.4	0.2±0.7*	0.6±0.4	3.6±0.4	0.7±0.5	1.1±0.3
ROI 5	8.7±0.3	0.2±0.8*	0.7±0.4	3.7±0.4	0.6±0.4	1.0±0.3

Unit cell vector length and average displacement (rms) from lattice in nm

Region	A [nm]	B [nm]	C [nm]	Volume [nm³]
ROI 1	14.0±0.5	14.4±0.6	10.2±0.7	2059
ROI 2	13.7±0.5	14.7±0.4	9.8±0.7	1978
ROI 3	13.7±0.6	15.2±0.4	10.0±0.6	2081
ROI 4	13.9±0.5	14.2±0.6	11.1±0.9	2187
ROI 5	13.8±0.5	13.9±0.7	11.2±0.7	2053

Unit cell vector angles in degrees

Region	AB [º]	BC [º]	CA [º]
ROI 1	92.3	89.9	93.4
ROI 2	88.8	89.7	89.7
ROI 3	91.8	90.4	88.2
ROI 4	93.8	92.3	87.4
ROI 5	96.2	90.9	106.1

Unit cell filling fractions (ρ) and size ratios (γ)

Region	ρ(d$_{core}$)	ρ(d$_{core}$+t$_{min}$)	ρ (d$_{core}$+t$_{3NN}$)	γ (d$_{core}$)	γ (d$_{core}$+t$_{min}$)	γ (d$_{core}$+t$_{3NN}$)
ROI 1	0.358	0.459	0.555	0.433	0.491	0.512
ROI 2	0.373	0.488	0.583	0.432	0.486	0.510
ROI 3	0.347	0.437	0.530	0.433	0.488	0.514
ROI 4	0.307	0.413	0.513	0.416	0.479	0.502
ROI 5	0.331	0.435	0.543	0.422	0.483	0.500

* A negative minimum neighbor distance (t$_{min}$) which could be interpreted as penetration of the NC hard cores is unphysical. Instead it results from analyzing NC as spherical objects which only approximates the actual shape of a faceted crystallite.

SI Table 4 ET analysis of AB consisting of PbSe and Au NCs.

Particle size distribution and shell thickness (normal distribution) in nm

Region	PbSe d_{core}	PbSe t_{min}	PbSe t_{3NN}	Au d_{core}	Au t_{min}	Au t_{3NN}
ROI 1	6.8±0.5	0.5±0.6*	1.0±0.5	4.6±0.4	1.3±0.3	1.6±0.3
ROI 2	6.8±0.4	0.5±0.6*	1.0±0.5	4.6±0.4	1.3±0.3	1.6±0.3
ROI 3	6.9±0.4	0.2±0.4*	0.6±0.3	4.6±0.4	1.3±0.3	1.6±0.2
ROI 4	6.9±0.4	0.6±0.6*	1.0±0.5	4.4±0.5	1.2±0.4	1.6±0.4

Unit cell vector length and average displacement (rms) from lattice in nm

Region	A [nm]	B [nm]	C [nm]	Volume [nm³]
ROI 1	10.9±0.6	10.4±0.5	10.5±0.6	1187
ROI 2	10.6±0.6	10.5±0.5	10.6±0.7	1175
ROI 3	10.7±0.4	10.8±0.4	10.5±0.4	1222
ROI 4	10.4±0.7	10.4±0.4	11.0±0.6	1174

Unit cell vector angles in degrees

Region	AB [°]	BC [°]	CA [°]
ROI 1	90.2	89.6	88.0
ROI 2	91.3	86.6	88.8
ROI 3	91.1	91.3	90.0
ROI 4	91.5	91.2	97.4

Unit cell filling fractions (ρ) and size ratios (γ)

Region	$\rho(d_{core})$	$\rho(d_{core}+t_{min})$	$\rho(d_{core}+t_{3NN})$	$\gamma(d_{core})$	$\gamma(d_{core}+t_{min})$	$\gamma(d_{core}+t_{3NN})$
ROI 1	0.224	0.353	0.420	0.682	0.824	0.808
ROI 2	0.226	0.352	0.420	0.670	0.797	0.791
ROI 3	0.224	0.332	0.384	0.662	0.824	0.813
ROI 4	0.221	0.345	0.410	0.647	0.765	0.768

PbSe and Au in face centered positions (mean±std) in unit cell of ROI 3
expressed in multiples of A,B,C

	A	B	C
Au 1	0.02±0.04	0.50±0.03	0.53±0.04
Au 2	0.48±0.05	0.49±0.03	1.00±0.05
Au 3	0.98±0.05	0.49±0.03	0.53±0.05
Au 4	0.49±0.04	0.50±0.03	0.05±0.05
PbSe 1	0.50±0.05	1.00±0.03	0.51±0.05
PbSe 2	0.50±0.05	0.01±0.03	0.51±0.03

* A negative minimum neighbor distance (t_{min}) which could be interpreted as penetration of the NC hard cores is unphysical. Instead it results from analyzing NC as spherical objects which only approximates the actual shape of a faceted crystallite.